Egypt. J. Chem. **Vol. 67**, No. 5 pp. 361 - 373 (2024)

Egyptian Journal of Chemistry

http://ejchem.journals.ekb.eg/

Copper Oxide Nanoparticles As A Promising Therapy For Modulating Ehrlich Ascitic Carcinoma And Promoting Foxo3a In Female Albino Mice

Wafaa K. Abo-Ghaneima [a]*, Wafaa M. Ibrahim [b], Sanaa M. Emam [a], Walaa A. Kishk [b]

[a] *Chemistry Department, Faculty of Science, Menoufia University, Menoufia, Egypt*

[b] *Department of Medical Biochemistry and Molecular Biology, Faculty of Medicine, Tanta University, Tanta, Egypt*

Abstract

Cancer is one of the most challenging health problems with many therapeutics are tried to combat it as nanomedicine. The present study aimed to investigate the potential antitumor effect of CuO NPs on the Ehrlich ascetic carcinoma (EC) model. To accomplish the objective, recent synthetic methods along with the characterization of CuO NPs were exploited. 90 female albino mice were involved and randomly divided into 6 equal groups: divided into Control, untreated group (EC) and treated Groups. The ascetic fluid from cancer groups and tissues from the control group were homogenized and used for the assay GADPH and mitochondrial F1 beta subunit of ATP synthase level. Forkhead transcription factor Oa3 (FOXOa3) gene expression, and nitric oxide level. The results obtained showed a notable improvement in mean survival time and cell viability, F1 beta subunit and FOXOa3 expression in the groups treated with CuO NPs, especially those receiving 10/2d mg/kg. Meanwhile, GAPDH and NO levels were decreased compared to the EC group. In conclusion; CuO NPs possess an antitumor effect by improving the bioenergetics signature.

Keywords: Copper oxide nanoparticles (CuO NPs); Ehrlich ascetic carcinoma (EC); Forkhead transcription factor Oa3 (FOXOa3); glyceraldehyde 3-phosphate dehydrogenase (GAPDH)

1. Introduction

Cancer is genetic alterations in the "cancer driver" genes, which can be caused by endogenous DNA replication errors or environmental mutagens [1]. Metabolic pathways and energy production abnormalities vary between normal and malignant cells. Genomic instability, persistent inflammation, and immune evasion are typically combined with metabolic reprogramming to promote tumor growth [2]. The Warburg effect explains metabolic regulation and the demand for cancer proliferation [3]. Cancer cells inhibit oxidative phosphorylation and rely primarily on anaerobic glycolysis, resulting in decreased ATP production and increased lactate production, which is used for many metabolic pathways responsible for biomass increase and metastasis, cancer cells rely on this low-energy pathway since it provides the carbon cytoskeleton for many metabolic intermediates like glutamate and fatty acid synthesis, which are both required for cellular component synthesis [4].

The bioenergetic signature was proposed to measure the main metabolic enzymes based on the metabolic hallmark of cancer cells. The bioenergetics signature is the ratio of the F1 beta subunit of ATP synthase to glyceraldehyde 3phosphate dehydrogenase (GAPDH). It is a tumor progression biomarker as well as a marker for cancer metabolism and responsiveness to treatment [5]. S-nitrosylation is a key element in how NO-based cellular signals are transferred during important cellular processes like transcription regulation, DNA repair, and apoptosis [6]. It was reported that excessive NO production can contribute to these pathological processes, specifically by S-nitrosylation of specific target proteins [7].

Forkhead container O proteins (FOXOs) are a class of transcription factors having 100 amino acid residues that bind to a variety of protein sequences [8]. FOXOs are capable of detecting changes in both intracellular and extracellular settings, and various stress signaling pathways as well as growth factors have an impact on their activity [9]. DNA repair, cell

*Corresponding author e-mail: wafaakhalid20@gmail.com

Receive Date: 14 July 2023, Revise Date: 25 October 2023, Accept Date: 07 November 2023

DOI: 10.21608/EJCHEM.2023.222975.8260

cycle arrest, and oxidative stress resistance are three functions of FOXOs, which are also known as tumor suppressors [10]. A tumor suppressor gene called FoxO3a is expressed in several organs [11].

Due to their nano-scale size, which permits better treatment effectiveness and long-term drug releases, Nanoparticles are sometimes referred to as structured contemporary pharmaceuticals that are particularly beneficial in treating cancer [12]. Metal nanoparticles generate free radicals that destroy cancer cells and dampen the tumor microenvironment. Tumor growth was slowed by the antioxidant properties of metal nanoparticles such as CuONP [13]. Nanoparticles can quickly enter cancer cells where they can kill them. In the dynamic procedure, nanoparticles are generated in a way that makes them specific to the malignant cell. Recent research illustrated that nanoparticles selectively attack cancer cells [14].

In the present study, Ehrlich ascetic carcinoma (EC) was used as an experimental animal model in this investigation. EC is a mouse mammary cancer that develops spontaneously and has been used in research.

To achieve the goal of this study, we assessed the level of the F1 beta subunit of ATP synthase and GAPDH, FOXOa3 as biomarkers in the EC model, as well as metabolic product nitric oxide and the effect of CuO NPs on this biomarker.

2. Material and Methode Reagents

Chemicals were purchased from Sigma-Aldrich Chemical Co., St. Louis, MO, USA except CuONP was prepared manually at (Menofya University, Faculty of Science).

2.1. CuO NPs preparation

Surfactants, starting precursors, and temperature modify the desired nanoparticle's shape and size [15]. By using green synthesis, the decomposition reaction taking place in the presence of heat is termed a thermal decomposition reaction. High temperatures help in breaking down the reactant into further molecules. When copper nitrate crystals are heated, they undergo a decomposition reaction to give copper oxide and nitrogen dioxide. The number of atoms is the same on the reactant and product sides.

$$Cu(NO_3)_2(s) \xrightarrow{\Delta} 2CuO(s) + 4NO_2 + O_2$$

2.2. Characterization of CuONP

2.2.1. X-ray Diffraction analysis (XRD)

An 18-Kw diffractometer with a monochromatic diffractometer (Bruker; model D 8 Advance) was used to gather X-ray diffraction (XRD) patterns in the scanning range of 5-90° (2θ) Cu-K radiation (λ= 1.54178 A°). Tanta Research Institute, Tanta, Egypt

2.2.2. The Fourier transform infrared spectrometer (FT-IR)

The spectroscopy FT-IR is exploited for identifying compounds and clarifying their structure utilizing (Neneyeus Nicoliditee 640 MSAFT-IR), and the standard KBr pellets at 400–4000 cm^{-1}, FT-IR spectra of the region, Tanta Research Institute, Tanta, Egypt.

2.2.3. The High-resolution transmission electron microscope (HR-TEM)

Tecnai G2 software and a High-Resolution Transmission Electron Microscope (HR-TEM) (FEI TECNAI 02) were used to capture the images. Using a (Gatan digital camera Erlangshen ES500) and a (JOEL JEM-M2100) operating at 200 kV, the HR-TEM experiment was carried out at the National Research Centre, Dokki, Giza, Egypt.

2.3. Experiment design

In the current study, 90 female albino mice weighed between 20 and 25 g. Their ages were between 6 and 8 weeks old and divided into 6 groups each group containing **(n =15)**. Mice received regular chew and had full access to food and water. Animal care and experimental methods were conducted at the Medical Biochemistry Department of Tanta University in Egypt. The animals were placed in wire mesh cages with a standard humidity (55%± 5%), a temperature of 23 °C, and a 12-hour light/dark cycle under the direction of the Menofya University in Egypt's Faculty of science ethical committee, **(Application code: SBio523)**

Group I (control group): Mice received intraperitoneal injections of saline at a dose of 100 µl for each, **Group II Cu 20/2d (Copper oxide NP 20 mg treated group):** CuO NPs were administered intraperitoneally to mice every other day for 14 days at a dose of 20 mg/kg body weight, **Group III (EC):** Mice received intraperitoneal injection of 100 µl of ascetic fluid containing $1*10^6$ Ehrlich cell control group (EC). Day zero was designated as the day of

the first injection. **Group IV (EC + CuO NPs 10/d)** Mice-bearing EACs received intraperitoneal injections of CuO NPs at a daily dose of 10 mg per kilogram of body weight for 14 days. **Group V (EC + CuO NPs 10/2d):** Mice-bearing EC received intraperitoneal injections of CuO NPs at 10 mg/kg of body weight every other day for 14 days. **Group VI (EC + CuO NPs 20/2d)** Mice-bearing ECs received intraperitoneal injections of CuO NPs at a dose of 20 mg/Kg body weight given every other day for 14 days. [16]

2.3.1. ***Specimen preparation***

At the experiment, the mice were euthanized and dissected while being just mildly drugged with ether. The mammary glands were then dissected and the extra saline was wiped using gauze. The peritoneal fluid was removed from the peritoneal cavity using a syringe (5 cm^3). The volume was determined by putting it in a graded centrifuge tube. The tumor cells were counted using a Neubauer hemocytometer and the total viable and non-viable EC were counted using the trypan blue exclusion method.

All groups, except group I control and group II CuO NP 20/2d, employed this procedure.

To obtain the cell deposit, the peritoneal fluid was collected and divided into four parts:

One part of the cell deposit was homogenized in phosphate buffer saline (pH=7.4) for Cytosolic GAPDH, The second half of the cell deposit was homogenized in mitochondrial isolation for Mitochondrial F1 Beta subunit of ATP synthase [16]. The third part was for NO by colorimetric method, The fourth part was for the detection of mRNA expressions of FOXOa3 using RT- PCR

2.3.2. Assessment of F1 Beta subunit of ATP synthase and GAPDH using enzyme-linked immunosorbent assay (ELISA)

The levels of GAPDH in the ascetic cell and mammary gland homogenate were determined by ELISA using a commercially available kit obtained from SunRed Biological Technology Company, Ltd, Shanghai. China.

The levels of the F1 Beta subunit of ATP synthase in the mitochondrial compartment of the ascetic cells and mammary gland homogenate were determined by ELISA using a commercially available kit obtained from SunRed Biological Technology Company, Ltd, Shanghai. China. The bioenergetics signature ratio was calculated through the equation (β-F1-ATPase/GAPDH) [17]

2.3.3. ***Assessment of nitric oxide (NO):*** *was determined according to [18].*

2.3.4**Assessment of FOXOa3 gene expression by real-time polymerase chain reaction (RT-PCR):**

Quantitative Real-time PCR (qRT-PCR) with German QIAGEN Rotor-Gene (Q5 plex) was used to measure the expression of mRNAs of target genes in the mammary gland in control and tumor cell pallet with β-actin as an internal reference.

Gene Expression Omnibus (http://www.ncbi.nlm.nih.gov/geo/query/acc.cgi?acc =GSE 135479). Reverse transcription and real-time PCR Reverse transcription and real-time PCR were performed as previously described [19]. DNA-free RNA was obtained with the RNeasy purification kit (Thermo Scientific, Fermentas, K0731).) with DNase treatment, and 1 mg of total RNA was reverse transcribed using a First Strand cDNA Synthesis Kit (the Fermentas, Thermo Scientific, Revert Aid H minus Reverse Transcriptase kit, #EP 0451), according to the manufacturer's instructions. Real-time PCR was done in triplicate with the QuantStudio5 Real-time PCR System and Fast SYBR Green Master Mix (ThermoFisher Scientific).

The Sequence **5' - 3 '**of FOXOa3 Forward (**CATGGACGACCTGCTGGATAACATC)** and Reverse Primer (**GAC GCA AGG AGTT CAGA GAC GAAG).**

In vitro gene silencing by small interfering RNAs

In vitro gene silencing by small interfering RNAs (siRNAs) was performed as previously described (20). Briefly, siRNAs targeting Foxo3 or their corresponding control oligos (80 nM) were transfected into murine BMMs using TransIT-TKO transfection reagent (Mirus Bio), in accordance with the manufacturer's instructions.

RNA sequencing and bioinformatics analysis RNA sequencing (RNA-seq) and bioinformatics analysis were performed as previously described (24). Briefly, total RNA was extracted using RNeasy Mini Kit (QIAGEN) following the manufacturer's instructions. TruSeq RNA Library preparation kits (Illumina) were used to purify poly-A+transcripts and generate libraries with multiplexed barcode adaptors, following the manufacturer's instructions. All samples passed quality control analysis using a Bioanalyzer 2100 (Agilent Technologies). RNA-seq

libraries were constructed per the Illumina TruSeq RNA sample preparation kit. Highthroughput sequencing was performed using the Illumina HiSeq 4000 in the Weill Cornell Medical College Genomics Resources Core Facility. RNA-seq reads were aligned to the mouse genome (mm10) using TopHat (25). Cufflinks (26) was subsequently used to assemble the aligned reads into transcripts and then estimate the transcript abundances as reads per kilo base per million values. HTseq (27) was used to calculate raw reads counts, and edgeR (28) was used to calculate normalized counts as counts per million.

Heatmaps were generated by pheatmap package in R. RNA-seq data (accession no. GSE 135479) have been deposited in National Center for Biotechnology Information's Gene Expression Omnibus (http://www.ncbi.nlm.nih.gov/geo/query/acc.cgi?acc =GSE 135479).

Reverse transcription and real-time PCR Reverse transcription and real-time PCR were performed as previously described (24). DNA-free RNA was obtained with the RNeasy Mini Kit (no. 74106; QIAGEN, Valencia, CA) with DNase treatment, and 1 mgof In vitro gene silencing by small interfering RNAs In vitro gene silencing by small interfering RNAs (siRNAs) was performed as previously described (20). Briefly, siRNAs targeting Foxo3 or their corresponding control oligos (80 nM) were transfected into murine BMMs using TransIT-TKO transfection reagent (Mirus Bio), in accordance with the manufacturer's instructions.

RNA sequencing and bioinformatics analysis

RNA sequencing (RNA-seq) and bioinformatics analysis were performed as previously described (24). Briefly, total RNA was extracted using RNeasy Mini Kit (QIAGEN) following the manufacturer's instructions. TruSeq RNA Library preparation kits (Illumina) were used to purify poly-A+transcripts and generate libraries with multiplexed barcode adaptors, following the manufacturer's instructions. All samples passed quality control analysis using a Bioanalyzer 2100 (Agilent Technologies). RNA-seq libraries were constructed per the Illumina TruSeq RNA sample preparation kit. Highthroughput sequencing was performed using the Illumina HiSeq 4000 in the Weill Cornell Medical College Genomics Resources Core Facility. RNA seq reads were aligned to the mouse genome (mm10) using TopHat (25).

Cufflinks (26) was subsequently used to assemble the aligned reads into transcripts and then estimate the transcript abundances as reads per kilo base per million values. HTseq (27) was used to calculate raw reads counts, and edgeR (28) was used to calculate normalized counts as counts per million.

Heatmaps were generated by pheatmap package in R. RNA-seq data (accession no. GSE 135479) have been deposited in National Center for Biotechnology Information's Gene Expression Omnibus (http://www.ncbi.nlm.nih.gov/geo/query/acc.cgi?acc =GSE 135479).

Reverse transcription and real-time PCR Reverse transcription and real-time PCR were performed as previously described (24). DNA-free RNA was obtained with the RNeasy Mini Kit (no. 74106; QIAGEN, Valencia, CA) with DNase treatment, and 1 mgof In vitro gene silencing by small interfering RNAs In vitro gene silencing by small interfering RNAs (siRNAs) was performed as previously described (20). Briefly, siRNAs targeting Foxo3 or their corresponding control oligos (80 nM) were transfected into murine BMMs using TransIT-TKO transfection reagent (Mirus Bio), in accordance with the manufacturer's instructions.

RNA sequencing and bioinformatics analysis RNA sequencing (RNA-seq) and bioinformatics analysis were performed as previously described (24). Briefly, total RNA was extracted using RNeasy Mini Kit (QIAGEN) following the manufacturer's instructions. TruSeq RNA Library preparation kits (Illumina) were used to purify poly-A+transcripts and generate libraries with multiplexed barcode adaptors, following the manufacturer's instructions. All samples passed quality control analysis using a Bioanalyzer 2100 (Agilent Technologies). RNA-seq libraries were constructed per the Illumina TruSeq RNA sample preparation kit. Highthroughput sequencing was performed using the Illumina HiSeq 4000 in the Weill Cornell Medical College Genomics Resources Core Facility. RNAseq reads were aligned to the mouse genome (mm10) using TopHat (25).

Cufflinks (26) was subsequently used to assemble the aligned reads into transcripts and then estimate the transcript abundances as reads per kilo base per million values. HTseq (27) was used to calculate raw reads counts, and edgeR (28) was used to calculate normalized counts as counts per million.

Heatmaps were generated by pheatmap package in R. RNA-seq data (accession no. GSE 135479) have been deposited in National Center for Biotechnology Information's Gene Expression Omnibus (http://www.ncbi.nlm.nih.gov/geo/query/acc.cgi?acc =GSE 135479).

Reverse transcription and real-time PCR Reverse transcription and real-time PCR were performed as previously described (24). DNA-free RNA was obtained with the RNeasy Mini Kit (no. 74106; QIAGEN, Valencia, CA) with DNase treatment, and 1 mg of In vitro gene silencing by small interfering RNAs In vitro gene silencing by small interfering RNAs (siRNAs) was performed as previously described (20). Briefly, siRNAs targeting Foxo3 or their corresponding control oligos (80 nM) were transfected into murine BMMs using TransIT-TKO transfection reagent (Mirus Bio), in accordance with the manufacturer's instructions.

RNA sequencing and bioinformatics analysis

RNA sequencing (RNA-seq) and bioinformatics analysis were performed as previously described (24). Briefly, total RNA was extracted using RNeasy Mini Kit (QIAGEN) following the manufacturer's instructions. TruSeq RNA Library preparation kits (Illumina) were used to purify poly-A+transcripts and generate libraries with multiplexed barcode adaptors, following the manufacturer's instructions. All samples passed quality control analysis using a Bioanalyzer 2100 (Agilent Technologies). RNA-seq libraries were constructed per the Illumina TruSeq RNA sample preparation kit. Highthroughput sequencing was performed using the Illumina HiSeq 4000 in the Weill Cornell Medical College Genomics Resources Core Facility. RNA seq reads were aligned to the mouse genome (mm10) using TopHat (25).

Cufflinks (26) was subsequently used to assemble the aligned reads into transcripts and then estimate the transcript abundances as reads per kilo base per million values. HTseq (27) was used to calculate raw reads counts, and edgeR (28) was used to calculate normalized counts as counts per million.

Heatmaps were generated by pheatmap package in R. RNA-seq data (accession no. GSE 135479) have been deposited in National Center for Biotechnology Information's Gene Expression Omnibus (http://www.ncbi.nlm.nih.gov/geo/query/acc.cgi?acc =GSE 135479).

Reverse transcription and real-time PCR Reverse transcription and real-time PCR were performed as previously described (24). DNA-free RNA was obtained with the RNeasy Mini Kit (no. 74106; QIAGEN, Valencia, CA) with DNase treatment, and 1 mg of In vitro gene silencing by small interfering RNAs In vitro gene silencing by small interfering RNAs (siRNAs) was performed as previously described (20). Briefly, siRNAs targeting Foxo3 or their corresponding control oligos (80 nM) were transfected into murine BMMs using TransIT-TKO transfection reagent (Mirus Bio), in accordance with the manufacturer's instructions.

RNA sequencing and bioinformatics analysis RNA sequencing (RNA-seq) and bioinformatics analysis were performed as previously described (24). Briefly, total RNA was extracted using RNeasy Mini Kit (QIAGEN) following the manufacturer's instructions. TruSeq RNA Library preparation kits (Illumina) were used to purify poly-A+ transcripts and generate libraries with multiplexed barcode adaptors, following the manufacturer's instructions. All samples passed quality control analysis using a Bioanalyzer 2100 (Agilent Technologies). RNA-seq libraries were constructed per the Illumina TruSeq RNA sample preparation kit. Highthroughput sequencing was performed using the Illumina HiSeq 4000 in the Weill Cornell Medical College Genomics Resources Core Facility. RNAseq reads were aligned to the mouse genome (mm10) using TopHat (25).

Cufflinks (26) was subsequently used to assemble the aligned reads into transcripts and then estimate the transcript abundances as reads per kilo base per million values. HTseq (27) was used to calculate raw reads counts, and edgeR (28) was used to calculate normalized counts as counts per million. Heatmaps were generated by pheatmap package in R. RNA-seq data (accession no. GSE 135479) have been deposited in National Center for Biotechnology Information's Gene Expression Omnibus (http://www.ncbi.nlm.nih.gov/geo/query/acc.cgi?acc =GSE 135479).

Reverse transcription and real-time PCR

Reverse transcription and real-time PCR were performed as previously described (24). DNA-free RNA was obtained with the RNeasy Mini Kit (no. 74106; QIAGEN, Valencia, CA) with DNase treatment, and 1 mg of The sequence of β- actin forward (**GCAGATGTGGATCAGCAAGC)** and reverse primers (**AGCTC AGTAA CAG TCCGCC**). The cycling condition was the following: the initial step of activation at 95C° for 5s,

followed by 40 cycles of denaturation at 95C° for 5 s, annealing at 60C° for 10s, and extension at 72 C° for 20 s. at the last cycle end, the temperature was increased from 63 C° to 95 C° for melting curve analysis

3. Statistical analysis

The collected data were statistically analyzed using graph pad Prism version 7. The mean and standard deviation A one-way analysis of variance (ANOVA) analysis of variance, and *post-hoc Dunn-Bonferroni* test were all performed. P-values under 0.05 were regarded as significant.

4. Result & Discussion

Cancers are a group of diseases characterized by the uncontrolled proliferation and spread of abnormal cells [20]. Breast cancer is one of the deadliest diseases that affect women [21]. According to published reports, existing chemotherapy medications have many drawbacks such as high cost, perniciousness, and significant side effects. So alternative therapeutics such as nano-drugs, and nano-formulations for drug delivery are critical. Copper is a well-known hazardous heavy metal to mammalian cells. Despite the fact that copper compounds have a high medicinal potential. The primary indicator that influences the toxicological consequences of Cu NPs is their exposure route. Cu NPs, due to their small size, can easily translocate between cells, and eventually reach the blood circulatory system. The circulatory and lymphatic systems play a crucial role in the transportation of NPs from the exposure site to downstream effects [15]

4.1. X-ray diffraction pattern analysis (XRD)

The crystal size of both modified and unmodified NPs was determined using the Debye-Scherrer equation.

$D = K\lambda/\beta\cos\theta$ [22]

D is the particle diameter in nanometers, K is the correction factor based on the crystallite's gyration radius is the X-ray radiation length of wavelength, β is the full width at half maximum (FWHM) in radians, and is the Bragg's diffraction angle. K is constant and equals the used X-ray radiation wavelength (1.54056 A°). The NPs' XRD pattern was compared to a Monoclinic CuO database from the Joint Powder Diffraction Joint Committee (PDF Card No. 01-080-1916) [23].

XRD peaks of green-synthesized CuO NPs with diffraction angles of 35.51, 38.96, 48.74, 58.22, 61.51, and 66.21° represented (h, k, l) values of reflection from crystal planes (-111), (111), (202), and (-113). The average particle size was 22.95nm, according to the XRD pattern.

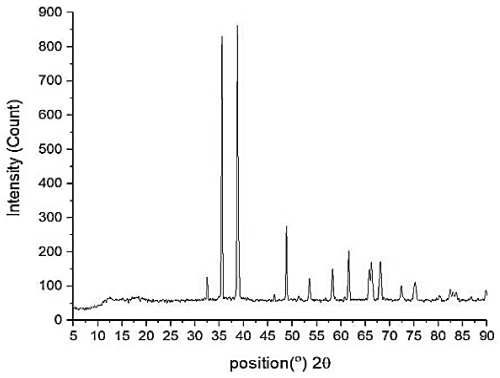

Figure 1: Show XRD of CuONP

4.2. Fourier transform infrared analysis (FT-IR)

The FTIR spectrum depicted in Figure 2 reveals strong and extensive absorption bands at 700 and 375 cm^{-1} indicated CuO. The FTIR spectra also indicated H_2O an absorption band at 3350 cm^{-1}[24].

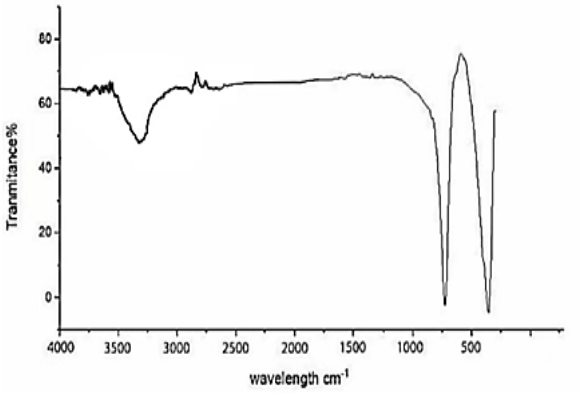

Figure 2: FT-IR spectrum of CuO-NPs

4.3. High-resolution transmission electron microscopy TEM

The CuONPs TEM picture indicated that the particles are almost spherical with only a slight thickness difference. The typical particle size, as revealed by the histogram, was between 200 and 500 nm [25].

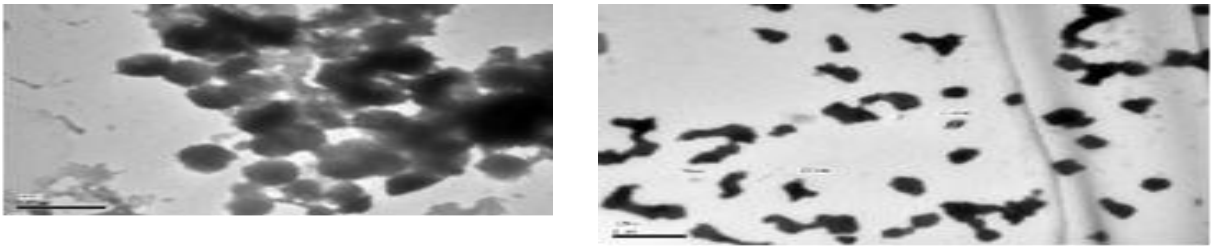

Figure 3: TEM image of CuO-NP

4.4. Experimental model, biochemical, and molecular study results

Our study consists of six groups; each group has 15 female albino mice. The groups are as the following C [saline-treated mice (20µl/kg I.P.)] for 14 days, EC [untreated Ehrlich ascetic carcinoma-bearing mice], CCuONP 20/ 2d [CuONP-treated mice (20mg/kg I.P. starting day 1)] for 14 days. for 14 days, ECuO 10 /d [EC bearing mice were given 10 mg of CuO NP every day beginning on day 1], ECuO 10/ 2 d [EC bearing mice were given 10 mg of CuO NP every other day beginning on day 1], ECuONP 20 /2d [EC bearing mice were given 20 mg of CuO NP every day beginning on day 1]. Five mice from each group were left and followed up till the time of their death. They were used for mortality calculation mean survival time.

The effect of CuO NPs on the MST, cell viability, and Ascetic fluid in EC groups

Table 1 shows the effect of CuONP on MST, cell viability, and ascetic volume in EC mice, compared to other groups that underwent treatment, the Ehrlich control group (EC) demonstrated a notably reduced MST level. Additionally, according to current research findings, the treated CuONP group with a dosage of 10 mg every alternate day showed an extremely substantial rise in their MST levels. This observation may indicate the potential anticancer properties of CuONPs

Our result agreed with Sunil et al., (2013), reporting that MST in Ehrlich Carcinoma was significantly decreased when compared to cisplatin [26] In addition to our result agreed with Morsy et al., (2020), reporting that ZnONP significantly increases among treatment groups of EC [16].

The study demonstrated a considerable reduction in th e count of viable cells and the percentage of cell viability after treating EC. Conversely, there was an observable increase in dead cells among treated EC compared to untreated ones, which had statistical significance. Notably, ECCuO 10/2d exhibited the most substantial decrease in both cell viability and percentage while showing an elevation in dead cells

Our result was in agreement with Shafagh et al., (2015): who reported that CuO nanoparticles induce cytotoxicity and apoptosis in the human K562 cancer cell line via the mitochondrial pathway [27], through reactive oxygen species and P53. Nagajyothi et al., (2017), also revealed that In-vitro anticancer results indicated that CuO NPs induced intracellular ROS generation in a dose-dependent manner and significantly reduced cervical carcinoma colonies [28]. Mohamed et al., (2021) reported that the percent of cell viability decreases as the concentration of CuONP rises [29].

By demonstrating that CuO NPs promoted apoptosis in cancer cells but not normal cells through the MTT experiment, Shafagh et al., 2015 demonstrated the unique effects of CuO NPs on cell viability [27]. Therefore, it is possible that a crucial mechanism behind the death of K562 cells is the regulation of P53 and Bax/Bcl2.

According to Kukia et al. (2018), an increase in the concentration of CuO nanoparticles resulted in a decrease in cell viability and an increase in apoptosis. Nevertheless, there were no notable differences observed between the two particle sizes (30 and 60 nm) at concentrations ranging from 10 to 20 µg/ml [30].

Benguigui et al. (2019) disclosed that metal oxide nanoparticles exhibit remarkable efficacy, particularly CuO-NPs which demonstrate potential as a novel therapeutic modality for pancreatic cancer [31]. Additionally, Wang et al. (2017) presented findings indicating the ability of CuONPs to selectively induce apoptosis and hinder the growth of malignant cells both in vitro and in vivo without detrimental effects on normal prostate epithelial cells [32], furthermore, these particles are capable of suppressing the stemness properties within cancer cells and obstructing the Wnt signaling pathway.

Furthermore, research indicates selective apoptotic induction of melanoma cells by CuONPs with negligible renal or hepatic toxicity concerns According to research conducted on mice, CuONP demonstrates the ability to impede tumor progression in pancreatic cancer. The tumors derived from subjects that underwent CuONP treatment exhibited a noticeably elevated quantity of apoptotic tumor-initiating cells (TICs) compared to those observed in untreated counterparts [27].

Melanoma development and metastasis inhibition by CuONPs in tumor-bearing mice models, with quick clearance by mice and low toxicity. CuONPs have outstanding anti-tumor qualities and are a good candidate to develop and create a novel anti-tumor medicine because they target the mitochondria and induce apoptosis of cancer cells by launching the mitochondrion-mediated apoptosis signaling pathway [33].

Table 1: MST, Dead cell, cell viability %, and ascetic volume in EC groups

Groups	MST	Cell viability %	Ascetic volume ($X10^6$ per ml)	Cell viability %
Group I control (n=5)	35±3.5 [c,d,e]	----------	----------	----------
Group II C CuO 20 2d (n=5)	33±3.55) [c,d,e]	----------	----------	----------
Group III EC (n=5)	15±2.55 [a,b,f]	40.4 % [d,e,f]	5.92±0.15 [d,e,f]	40.4 % [d,e,f]
Group IV EC CuO 20 2 d (n=5)	22±2.53 [c]	28.6 % [c,e,f]	3.92±0.09 [c,d,f]	28.6 % [c,e,f]
Group V EC CuO 10 d (n=5)	20.5±2.45 [c]	18.6 % [c,d,f]	2.91±0.10 [c,d,f]	18.6 % [c,d,f]
Group VI EC CuO 10 2d (n=5)	30±3.44 [c,d,e]	12.2 % [c,d,f]	1.89±0.17 [c,d,f]	12.2 % [c,d,f]

Note: All data are expressed as mean and standard deviation.
Using the post hoc Dunn- Bonferroni test, significant difference with Significant $P < .05$.
[(a)] Control: Saline- treated mice,
[(b)] CCuO: 20mg/2d I.P. for 14 days,
[(c)] EC: untreated Ehrlich ascitic carcinoma
[(d)] ECuO 10/d: 10 mg/kg I.P. every day,
[(e)] ECuO 10/2d: 10 mg/kg I.P. every other day,
[(f)] ECuO 20/2d: 20 mg/kg I.P. every other day.
Abbreviations: MST, mean survival time; CuO NP, Copper oxide nanoparticle.

4.4.5. The effect of CuO NPs on the ATP Synthase, GADPH, bioenergetics signature, NO, and FOXOa3 of EC cells

Tables 2 show the effect of CuONP on EC mice in different treatment groups. The phenomenon known as the Warburg effect elucidates how metabolic regulation and necessities facilitate cancer proliferation. In particular, malignant cells curtail oxidative phosphorylation while relying primarily on anaerobic glycolysis to generate adenosine triphosphate (ATP), which yields fewer ATP molecules but more lactate that fuels various metabolic pathways and promotes biomass amplification and metastasis. Therefore, quick glucose consumption enables a steady stream of energy in even the most difficult environments [13].

The Warburg phenomenon had a significant impact on cancer development, leading to the introduction of the bioenergetics signature concept [34]. This biomarker relies on the F1 B subunit of ATP synthase and GAPDH ratio, where both serve as markers for oxidative phosphorylation and glycolysis pathways in relation to cancer diagnosis and treatment response assessment [35].

The glycolytic pathway is considered the hallmark pathway of cancer cells [36]. This pathway provides the cancerous cell with a rapid source of energy and different metabolic intermediate that in different synthetic pathways. The main upregulated glycolytic enzymes are hexokinase, phosphofructokinase-1, phosphofructokinase 2,6 bisphosphofructose, and bio function enzyme aldolase, GAPDH, and lactate dehydrogenase enzymes [37].

ATP Synthase is the other mainstay of the bioenergetics fingerprint. The majority of the ATP in a cell comes from F1Fo ATP synthases [38]. Since cancer's energy metabolism is now seen as a defining feature, researchers have begun looking into mitochondrial and glycolytic pathways. For example, F1-ATPase, a rate-limiting component of mitochondrial oxidative phosphorylation and a catalytic subunit of mitochondrial H^+-ATP synthase, is expressed much less in human tumors than in normal tissues [39].

We found that the F1 beta subunit of ATP synthase in EC was significantly lower in the CuONP-treated group compared to both the control group and the untreated group. Although the most recent findings dispelled any doubt, the F1 beta subunit was shown to be significantly higher in the treated ECs groups than in the ECs groups overall. The control group had the highest F1 beta ATP synthetase level, followed by the Control CuO 20 2d and the EC CuO 10 2d, with no significant difference between the Ehrlich CuO 10/d group and the ECuO 20/2d group over several days.

Our result was in accordance with Morsy et al., 2020 illustrating that F1 beta subunit of ATP, all groups had a significant increase of the F1 beta subunit of ATP synthase, relative to the untreated EC group. [16].

Also; many previous publications have reported altered or decreased mitochondrial ATP synthase in aggressive human cancers [40].

According to the current research, a substantial elevation of GAPDH was detected in the Ehrlich control group (EC) as opposed to other treated groups. In addition, the results indicated that CuONP demonstrated dose-dependent efficacy on GAPDH levels among these treated groups. Specifically, it was observed that administering 10 mg of CuONP every other day resulted in the most remarkable reduction of GAPDH levels within this cohort. This finding may suggest that CuONPs possess an anticancer potential against EC models.

Our result was in harmony with Morsy et al., (2020), reporting that GAPDH is the most commonly overexpressed enzyme in multiple types of cancers and therapeutic approaches, particularly breast cancer. Otherwise, there was found to inhibit cancer growth [16], so this could identify the role of bioenergetics signature biomarker of the glycolytic pathway. Also; Tarrado-Castellarnau et al., (2017); reported that GAPDH is increased in all stages of colorectal tumor progression [41].

Table 2: F1 ATP synthase GAPDH, Bioenergetics, Nitric oxide, FOXOa3

Groups	F1 beta subunit of ATP synthase (ng/mg protein) (n=5)	GAPDH **(ng/mg protein)** (n=5)	**Bioenergetics signature**	Nitric oxide **(µmol/ mg protein)** (n=5)	FOXOa3 (n=1)
Group I control (n=5)	0.45±0.03 [c,d,e]	0.15±0.01 [c,e]	3	0.60±0.11	1.0±0.03
Group II C CuO 20 2d (n=5)	0.42±0.03 [c,d,e]	0.17±0.01 [c,e]	2.4	0.64±0.15	0.85±0.08
Group III EC (n=5)	0.30±0.03 [a,b,f]	0.25±0.01 [a,b,d,f]	1.2	3.38±0.13	0.25±0.04
Group IV EC CuO 20 2 d (n=5)	0.33±0.02 [a,b,f]	0.19±0.01 [e]	1.7	3.20±0.07	0.5±0.04
Group V EC CuO 10 d (n=5)	0.33±0.02 [a,b,f]	0.20±0.01 [e]	1.6	0.88±0.35	0.6±0.05
Group VI EC CuO 10 2d (n=5)	0.40±0.04 [c,d,e]	0.18±0.01 [e]	2.22	0.77±0.11	0.8 ±0.06

Note: All data are expressed as mean and standard deviation.

Using the post hoc Dunn-Bonferroni test, significant difference with Significant $P < .05$.

(a) Control: Saline-treated mice,

(b) CCuO: 20mg/2d I.P. for 14 days,

(c) EC: untreated Ehrlich ascitic carcinoma

(d) ECuO 10/d: 10 mg/kg I.P. every day,

(e) ECuO 10/2d: 10 mg/kg I.P. every other day,

(f) ECuO 20/2d: 20 mg/kg I.P. every other day.

Abbreviations: NO: Nitric oxide, glyceraldehyde 3phosphate dehydrogenase: GAPDH,

NO is a transient signaling molecule found everywhere and involved in a wide variety of essential bodily processes. The effects of NO on carcinogenesis and tumor growth are controversial and the results have crucial implications for treatment. NO is a key factor in tumor development, progression, and spread [42].

Our data showed that compared to the control group of untreated ECs, nitric oxide levels dropped significantly. Nitric oxide level in EC was higher compared to the CuONPs-treated group and control group. Nitric oxide levels were found to be lowest in the ECuO 10 2d and ECuO 10 d groups, respectively.

Overall, NO has a "double-edged sword" when it comes to cancer. On the one hand, high levels of NO, which can be made by active macrophages, may cause cancer cells to die and stop the cancer from growing. On the other hand, (relatively) low levels of NO (such as levels that can be measured in many different types of clinical cancer samples) help tumors grow and spread. [42]

Fukumura et al., 2006: illustrate that Nitric oxide (NO) and nitric oxide synthases are ubiquitous in malignant tumors and are known to exert both pro- and anti-tumor effects. [43]

Liu et al., 1998; illustrated that iNOS activity was upregulated in alveolar macrophages of patients with primary lung cancer, leading to an increase in NO production. The increased NO production was not unique to the tumor side and may be attributable to non-specific immunological and inflammatory host processes associated with the tumor [44].

Our result was accepted by Nagajyothi et al., 2015 who suggested that ZnONP decreased the level of nitric oxide in cancer cells and has antioxidant properties. [45]

However, there were other studies that contradicted our results, it was revealed that CuONP can achieve high levels of Nitric oxide which consequently lead to oxidative stress and cellular damage. [46]

Hanley et al. 2009, observed that there is an inverse relationship between nanoparticle size and cytotoxicity in mammalian cells, as well as nanoparticle size and reactive oxygen species production.[47], GAPDH was confirmed to be linked to iNOS in cells by Chakravarti et al., 2010 [48].

Our data showed that the expression of FOXOa3 in ECs was significantly lower compared to control and CuONP-treated groups. Recent studies have shown that across all groups, ECuO 10 2d had the highest levels of FOXOa3. Significantly higher levels of FOXOa3 were observed in CuO NP-treated groups.

Nuclear FOXOa3 expression in breast cancer cell models can result in cancer progression and the development of an aggressive phenotype similar to that seen in cytotoxic chemotherapy-resistant breast cancer cell models, as well as significantly reducing their response to tamoxifen and cytotoxic chemotherapy [49].

Nuclear FOXOa3 translocation also triggered antioxidant gene transcription and protected cells from oxidative damage [50]. Previous studies reported the overexpression of FOXOa3 inhibited tumor growth *in vitro* and also reduced tumor size *in vivo* in breast cancer [51].

Khan et al., 2022 represented the downregulation of FOXOa3 in breast cancer. The relationship between decreased FOXOa3 expression and advanced breast cancer stages may serve as a prognostic biomarker [52].

According to Han et al. (2020), titanium dioxide TiO_2 induced p-FOXOa3/FOXOa3 activation in rat lungs, livers, and kidneys in a dose-dependent manner. DNA damage was dramatically elevated in the liver, kidneys, and lungs of those given Nano-TiO_2, and it did not repair itself after 7 days. These findings suggested that activation of the PI3K-AKT FOXOa3 signaling pathway may be related to DNA damage generated by NanoTiO_2 [53].

5. Conclusion

Our results indicated that CuO NPs have a significant efficiency against cancer cells via an effect on significantly reduced mean survival, cell viability, ascetic volume, GAPDH, and NO while significantly increasing ATP synthase, Bioenergetics signature, and FOXOa3. This encouraging result provides useful information for designing a much better anticancer compound using a plant-mediated synthesis of CuO

results described elsewhere in the article. Please avoid using vertical rules and shading in table cells.

6. Reference

[1] Balmain A., (2020); The critical roles of somatic mutations and environmental tumor-promoting agents in cancer risk. Nat. Genet. 52, 1139–1143.

[2] Hanahan D., and Weinberg R. A., (2011); Hallmarks of cancer: The next generation. Cell 144, 646–674.

[3] Liberti M. V., Locasale J. W. (2016); The Warburg Effect: How Does it Benefit Cancer Cells. Trends Biochem. Sci., 41, 211.

[4] Xie J., Wu H., Dai C., Pan Q., Ding Z., Hu D., Ji B., Luo Y., Hu X. (2014); Beyond Warburg effect--dual metabolic nature of cancer cells Sci. Rep. 4, 4927.

[5] Cuezva J.M., Krajewska M., De-Heredia M.L., Krajewski S., Santamaría G., Kim H., Zapata J. M., Marusawa H., Chamorro M., and Reed J. C., (2002); The bioenergetic signature of cancer: a marker of tumor progression. Cancer Res. 62, 6674-6681.

[6] Wang Z. (2012); Protein S-nitrosylation and cancer. Cancer Letters 320, 123-129

[7] Nakamura T. and Lipton S.A. (2011); S-Nitrosylation of Critical Protein Thiols Mediates Protein Misfolding and Mitochondrial Dysfunction in Neurodegenerative Diseases. Antioxid Redox Signal. 14, 1479–1492.

[8] Kaestner K. H., Knochel W., and Martinez D. E., (2000); Unified nomenclature for the winged helix/forkhead transcription factors. Genes Dev. 14, 142–146.

[9] Eijkelenboom A., and Burgering B. M. T., (2013); FOXOs: signaling integrators for homeostasis maintenance. Nat. Rev. Mol. Cell Biol. 14, 83–97.

[10] Zhang Y., Gan B., Liu D., and Paik J.-H., (2011); FOXO family members in cancer. Cancer Biol. Ther. 12, 253–259.

[11] Yu T., Ji J., Guo Y.-L., (2013); MST1 activation by curcumin mediates JNK activation, Foxo3a nuclear translocation, and apoptosis in melanoma cells. Biochem. Biophys. Res. Commun. 441, 53–58.

[12] Roopan S.M., Bharathi A., Kumar R., Khanna V.G., Prabhakarn A. (2012); Agricultural waste Annona squamosa peel extract: biosynthesis of silver nanoparticles, Colloid. Surf. B. 92, 209–212.

[13] Naz S., Gul A., and Zia M., (2020); Toxicity of copper oxide nanoparticles: a review study. IET Nanobiotechnol. 14, 1-13

[14] Danhier F., Feron O. and Préat V. (2010); To exploit the tumor microenvironment: passive and active tumor targeting of nanocarriers for anti-cancer drug delivery. Journal of controlled release, 148, 135-146.

[15] Naz S., Gul A., Zia M. and Javed R. (2023); Synthesis, biomedical applications, and toxicity of CuO nanoparticles. Appl Microbiol Biotechnol. 107, 1039–1061.

[16] Morsy S., Abd- El latif R.N., Soliman N.A., Ibrahim W.M. (2020); Bioenergetic signature as a target of zinc oxide nanoparticles in Ehrlich ascitic carcinoma- bearing mice. J Biochem Mol Toxicol. 35, 1-7

[17] Strober W. (2015); Trypan Blue Exclusion Test of Cell Viability. Curr Protoc Immunol. 111, A3.B.1–A3.B.3.

[18] Giustarini D., Rossi R., Milzani A., and Dalle-Donne I. (2008); Nitrite and nitrate measurement by Griess reagent in human plasma: evaluation of interferences and standardization Methods Enzymol. 440, 361-380

[19] Sadaf, Habib M, Khan MA, Najm MZ, Mallick MN, Sunita K, et al.. (2018); Hypermethylated LATS2 gene with decreased expression in female breast cancer: A case control study from north India. Gene. 676, 156–63.

[20] Mathur G., Nain S. and Sharm P.K. (2015); Cancer: An Overview Academic Journal of Cancer Research 8 (1): 01-09

[21] Łukasiewicz S., Czeczelewski M., Forma A., Baj J., Sitarz R. and Stanisławek A. (2021); Breast Cancer Epidemiology, Risk Factors, Classification, Prognostic Markers, and Current Treatment Strategies An Updated Review. Cancers,13,1-30

[22] Jamdade D.A., Rajpali D., Joshi K.A., Kitture R., Kulkarni A.S., Shinde V.S., Ghosh S. (2019): Gnidia glauca-and plumbago zeylanica-mediated synthesis of novel CuONPs as promising antidiabetic agents, Adv.Pharmacol. Sci. 2019, 1-1

[23] Emam S.M. (2016): Spectral Characterization, Thermal and Biological Activity Studies of Schiff Base Complexes Derived from 4,4′-Methylenedianiline, Ethanol Amine and Benzil. J. Mol. Struct. 16, 1-9

[24] Silim H. A. (2005); FTIR Spectroscopy and Structure of the Binary Glass Cu2O – MoO3 System. Egypt. J. Solids.28, 16-23

[25] Mobarak M.B., Hossain M. S., Chowdhury F. and Ahmed S. (2022): Synthesis and characterization of CuO nanoparticles utilizing

waste fish scale and exploitation of XRD peak profile analysis for approximating the structural parameters. Arab. J. Chem. 15,1-18

[26] Sunil D., Isloor A.M., Shetty P., Nayak P.G. and Pai K.S.R. (2013); In vivo anticancer and histopathology studies of Schiff bases on Ehrlich ascitic carcinoma cells. Arab. J. Chem.6, 25-33

[27] Shafagh, M., Rahmani, F., and Delirezh, N., (2015); CuO nanoparticles induce cytotoxicity and apoptosis in human K562 cancer cell line via the mitochondrial pathway, through reactive oxygen species and P53. Iran. J. Basic Med. Sci. 18, 993–1000.

[28] Nagajyothi, P.C., Muthuramanb P., Sreekanthc T.V.M., Kim D.H., Shim J. (2017); Green synthesis: In-vitro anticancer activity of copper oxide nanoparticles against human cervical carcinoma cells. Arab. J. of Chem. 10, 1-11

[29] Mohamed R.M., Fawzy E.M., Shehab R.A., Ali D.M., Salah El D.R.A. and Abd El Fatah H.M. (2021); Green biosynthesis, structural characterization and anticancer activity of copper oxide nanoparticles from the brown alga Cystoseira myrica. EJABF. 25, 341 – 358

[30] Kukia N.R., Abbasi A. and Froushani S.M. A. (2018); Copper Oxide Nanoparticles Stimulate Cytotoxicity and Apoptosis in Glial Cancer Cell Line. Dhaka University Journal of Pharmaceutical Sciences 17, 105-111.

[31] Benguigui M., Weitz I. S., Timaner M., Kan T., Shechte D., Perlman O., Sivan S., Raviv Z., Azhari H. and Shaked Y. (2019); Copper oxide nanoparticles inhibit pancreatic tumor growth primarily by targeting tumor initiating cells Sci. Rep. 9, 1-10

[32] Wang Y., Yang Q.W., Yang Q., Zhou T., Shi M.F., Sun C.X., Gao X.X., Cheng Y.Q., Cui X.G. and Sun Y.H. (2017); Cuprous oxide nanoparticles inhibit prostate cancer by attenuating the stemness of cancer cells via inhibition of the Wnt signaling pathway. Int J Nanomedicine. 12: 2569–2579.

[33] Wang Y., Yang F., Zhang H.X., Zi X.Y., Pan X.H., Chen F., Luo W.D., Li J.X., Zhu H.Y. and Hu Y-P. (2013); Cuprous oxide nanoparticles inhibit the growth and metastasis of melanoma by targeting mitochondria. Cell Death and Disease 4, 1-10

[34] Pascale R.M., Calvisi D.F., Simile M.M., Feo C.F. and Feo F. (2020); The Warburg Effect 97 Years after Its Discovery. Cancers (Basel). 12, 1-33

[35] Ward PS. and Thompson CB. (2012); Metabolic reprogramming: a cancer hallmark even Warburg did not anticipate. J, of Cancer Cell 21, 297-308

[36] Sirover M.A. (2018); Pleiotropic effects of moonlighting glyceraldehyde-3-phosphate dehydrogenase (GAPDH) in cancer progression, invasiveness, and metastases. Cancer Metastasis Rev. 37, 665-676

[37] Kagawa Y. (2010); ATP synthase: from single molecule to human bioenergetics. Proc Jpn Acad Ser B Phys Biol Sci. 86, 667–693.

[38] Kalyanaraman B., Cheng G., Hardy M., Ouari O., Lopez M., Joseph J., Zielonka J. and Dwinell M.B. (2018); A review of the basics of mitochondrial bioenergetics, metabolism, and related signaling pathways in cancer cells: Therapeutic targeting of tumor mitochondria with lipophilic cationic compounds. Redox Biology 14. 316–327

[39] Zheng J. (2012); Energy metabolism of cancer: Glycolysis versus oxidative phosphorylation (Review). Oncol Lett. 1151–1157.

[40] Shin Y. K., Yoo B.C., Chang H.J, JeonE, Hong SH, Jung MS, et al. (2005); Down-regulation of mitochondrial F1F0-ATPsynthase in human colon cancer cells with induced5-fluorouracil resistance. Cancer Res.65,3162–3170.

[41] Tarrado-Castellarnau M., Diaz-Moralli1S., Polat I.H., Sanz-Pamplona R., Alenda C., Moreno V., Castells A. and Cascant M. (2017); Glyceraldehyde -3-phosphatedehydrogenase is overexpressed in colorectal cancer onset. transl med commun. 2, 1-9

[42] Xu W., Liu L.Z., Loizidou M., Ahmed M. and CharlesI.G. (2002); The role of nitric oxide in cancer. Cell Res. 12, 311–320

[43] Fukumura D., Kashiwagi S. and Jain R.K . (2006); The role of nitric oxide in tumour progression. Nat Rev Cancer 6,521-34

[44] Liu C-Y, Wang C-H, Chen T-C, Lin H-C, Yu C-T and Kuo H-P. (1998); Increased level of exhaled nitric oxide and up-regulation of inducible nitric oxide synthase in patients with primary lung cancer. British Journal of Cancer .78, 534–541

[45] Nagajyothi P. C , Cha S.J , Yang I. J Sreekanth T.V.M , Kim K.J. and Shin H.M. (2015); Antioxidant and anti-inflammatory activities of zinc oxide nanoparticles synthesized using Polygala tenuifolia root extract J Photochem Photobiol B.146:10-7

[46] Abdelazeim S.A., Shehata N.I, Aly H. F. and Shams S.G.E. (2020); Amelioration of oxidative stress-mediated apoptosis in copper oxide nanoparticles-induced liver injury in rats by potent antioxidants. Sci Rep. 10, 10812.

[47] Hanley C, Thurber A, Hanna C, Punnoose A, Zhang J, Wingett DG. (2009); The influences of cell type and ZnO nanoparticle size on immune cell cytotoxicity and cytokine induction. Nanoscale Res Lett. 4, 1409–1420.

[48] Chakravarti R., Aulak K.S., Fox P.L. and Stuehr D.J. (2010); GAPDH regulates cellular heme insertion into inducible nitric oxide synthase. Proc Natl Acad Sci. 107,18004-18009.

[49] Chen J, Gomes AR, Monteiro LJ, Wong SY, Wu LH, et al . (2010); Constitutively Nuclear FOXO3a Localization Predicts Poor Survival and Promotes Akt Phosphorylation in Breast Cancer. PLoSONE 5, 1-17

[50] Wang T., Zhang Z., Xie M., Li S., Zhang J. and Zho J. (2021); Apigenin Attenuates Mesoporous Silica Nanoparticles-Induced Nephrotoxicity by Activating FOXO3a. *Biological Trace Element Research* 200, 2793–2806

[51] Hu MC, Lee DF, Xia W, Golfman LS, Ou-Yang F, Yang JY, et al.. IkappaB kinase promotes tumorigenesis through inhibition of forkhead FOXO3a. *Cell* (2004) 117(2):225–37.

[52] Khan MA, Sadaf, Ahmad I, Aloliqi AA, Eisa AA, Najm MZ, Habib M, Mustafa S, Massey S, Malik Z, Sunita K, Pawar JS, Akhter N, Shukla NK, Deo SVS and Husain SA (2023)FOXO3 gene hypermethylation and its marked downregulation in breast cancer cases: A study on female patients. Front.Oncol.12, 1-20

[53] Han B., Pei Z., Shi L., Wang Q., Li C., Zhang B., Su X., Zhang N., Zhou L., Zhao B., Niu Y. and Zhang R. (2020); TiO2 Nanoparticles Caused DNA Damage in Lung and Extra-Pulmonary Organs Through ROS Activated FOXO3a Signaling Pathway After Intratracheal Administration in Rats International Journal of Nanomedicine 15, 6279-6294